frontiers in Materials

ORIGINAL RESEARCH
published: 08 March 2019
doi: 10.3389/fmats.2019.00031

Kinetic Insight on Improved Chemi-Resistive Response of Hydrothermal Synthesized Pt Loaded TiO_2 Nano-rods Toward Vapor Phase Isopropanol

Priyanka Das[1,2], *Biswanath Mondal*[1,2] *and Kalisadhan Mukherjee*[1,3]*

[1] Centre for Advanced Materials Processing, CSIR-Central Mechanical Engineering Research Institute, Durgapur, India, [2] Academy of Scientific and Innovative Research (AcSIR), CSIR-Central Mechanical Engineering Research Institute, Durgapur, India, [3] Department of Electrical and Computer Engineering, Science and Engineering Hall, Washington, DC, United States

Flower like microstructure composed of eccentrically grown vertically aligned titania nano-rods is prepared through spherical carbon template mediated hydrothermal route. Mechanistic pathways for the growth of said esthetic architecture is proposed by studying their phase formation behavior and morphological features. Chemi-resistive type sensing properties of prepared titania flowers for the detection of isopropanol are studied by varying the sensor operating temperature (225–300°C) and vapor concentration (10–200 ppm). Distinguishable sensitivity of titania flowers is identified for the detection of even 10 ppm isopropanol. Catalytic amount of Pt nano-particles (synthesized through chemical method) are introduced over prepared flower like titania to improve further their sensitivity. The plausible isopropanol sensing mechanism over TiO_2 flowers as well as influence of operating temperature and role of Pt nanoparticles as chemical sensitizer in enhancing the response is explained. The current response transients of both the TiO_2 flowers and their Pt modified counterpart for detecting low concentration (10–50 ppm) of isopropanol are modeled in accordance to Langmuir-Hinshelwood reaction mechanism and the rate constants for the respective surface reactions are estimated. The higher rate constant for the interaction of isopropanol over titania flowers than Pt modified counterparts is explained using the concept of decaying depleted layer during sensing.

Keywords: titania, morphology, nano-rod, gas sensor, noble metal, spill-over technique

OPEN ACCESS

Edited by:
Sheikh A. Akbar,
The Ohio State University,
United States

Reviewed by:
Priyanka Karnati,
The Ohio State University,
United States
Rodrigo Moreno,
Instituto de Cerámica y Vidrio (ICV),
Spain

***Correspondence:**
Kalisadhan Mukherjee
kalisadhanm@yahoo.com

Specialty section:
This article was submitted to Functional Ceramics, a section of the journal Frontiers in Materials

Received: *09 January 2019*
Accepted: *14 February 2019*
Published: *08 March 2019*

Citation:
Das P, Mondal B and Mukherjee K (2019) Kinetic Insight on Improved Chemi-Resistive Response of Hydrothermal Synthesized Pt Loaded TiO_2 Nano-rods Toward Vapor Phase Isopropanol. Front. Mater. 6:31. doi: 10.3389/fmats.2019.00031

INTRODUCTION

Titania (TiO_2) is an important semiconducting metal oxide (SMO) which remains attractive to the researchers for its high physicochemical stability, low toxicity and widespread applications in catalysis, gas sensors, Li-ion batteries, photo-splitting of water, photovoltaic devices etc. (O'Regan and Grätzel, 1991; Bai and Zhou, 2014; Schneider et al., 2014; Li et al., 2017; Zhou et al., 2017). In most of these applications, the performance of TiO_2 often significantly varies with its phase formation behavior and morphological features (Park et al., 2000; Yurdakal et al., 2008). Researchers have prepared various simple as well as complex architectures of TiO_2 for different applications (Wang et al., 2010; Damodaran et al., 2015). As evident from the literatures, syntheses

of these morphologies are generally carried out either using physical or chemical methods. Physical methods e.g., chemical vapor deposition (CVD), physical vapor deposition (PVD), molecular beam epitaxial (MBE) growth etc. are very popular for preparing fascinating homogeneous morphologies of SMOs including titania (Lao et al., 2002; Tian et al., 2003; Shi and Wang, 2011). However, the high investment and operational cost of these sophisticated instruments often limit their use in industries as well as R&D sectors. On contrary, chemical methods are cost effective and capable yet to prepare the SMOs in different nano/micron size architectures. Chemical methods (e.g., co-precipitation, auto-combustion etc.) are usually influenced by the precursor type as well as pH, temperature, pressure of the reaction media which as a whole changes the reaction kinetics and restricts obtaining desired morphology repetitively. On contrary, template mediated synthesis of hydrothermal/sol-gel methods are considered effective techniques to reproduce desired esthetically impressive architectures of SMOs in different batch reactions. For instance, anodized alumina template assisted wet chemical methods for the preparation of 1D SMO nano-structures are reported elsewhere (Lakshmi et al., 1997; Mao and Wong, 2004; Lee et al., 2011; Mukherjee and Majumder, 2013). Polysaccharide templates are used to fabricate SnO_2, Al_2O_3, TiO_2, CeO_2, ZrO_2 etc. metal oxide by Sun et al. (Sun et al., 2006). Titirici et al. has described the synthesis of Fe_2O_3, Co_3O_4, NiO hollow spheres using spherical carbon templates (Titirici et al., 2006). In the present work, flower like distinctive architecture composed of innumerable numbers of TiO_2 nano-rods is prepared through spherical carbon template mediated hydrothermal process. Phase, morphology, lattice fringe pattern and selected area electron diffraction patterns of the prepared TiO_2 are studied and a mechanistic pathway for the growth of said esthetic architecture is proposed. Chemi-resistive changes of TiO_2 flowers for the detection of isopropanol are studied using a static flow gas sensing measurement set-up developed in the laboratory. The sensitive detection of isopropanol using low cost sensors is demanding since this widely used solvent/reagent causes eye, nose, dermal irritation and critical central nervous system damage for animals (Jammalamadaka and Raissi, 2010). Prepared TiO_2 flowers can detect even 10 ppm isopropanol and the catalytic modification of these using Pt nano-particles can improve its sensitivity further. The nano-structured SMOs while are promising for the detection of toxic gases, catalytic modification using noble metals are attractive to make them more sensitive (Hotovy et al., 2004; Epifani et al., 2008; Hu et al., 2010; Wang et al., 2012; Bhowmik and Bhattacharyya, 2015). For instances, Wang et al. has reported ethanol sensing characteristics of Pd nanoparticle decorated TiO_2 nanobelts with improved sensitivity (Wang et al., 2012). Hotovy et al. shows the enhanced H_2 sensing characteristics of Pt modified NiO thin films as compared to its unmodified counterpart (Hotovy et al., 2004). Epifani et al. (2008) reports the effect of Pt on the H_2 sensitivity of anatase phase TiO_2 thin films. The sensing of isopropanol by primitive SMOs or their noble metal modified counterparts however nurtured by very few researchers (Dong et al., 2014). In this context, the cost effective synthesis of novel TiO_2 esthetic architecture, their catalytic modification using wet chemically synthesized Pt nano-particles, detail study on their phase and morphological features as well as operating temperature dependent isopropanol sensing characteristics could provide comprehensive insight to the researchers. The explanation on the role of Pt nanoparticles as chemical sensitizer in improving the sensitivity of TiO_2 is also important. Further, the current response transients of primitive and Pt modified TiO_2 are correlated with the sequential surface reactions operative for detection of isopropanol and modeled in accordance to Langmuir Hinshelwood reaction mechanism. The values of characteristic time constants (τ), rate constants (k_a) are estimated from the model and the underlying reasons for their differed values for primitive and Pt modified TiO_2 sensing elements are discussed.

EXPERIMENTAL

Synthesis of Materials

Synthesis of TiO_2 Flower Like Architecture (Ti-Nr)

The flow diagram for the synthesis of flower like architecture of TiO_2 nano-rods (Ti-Nr) is described in **Figure 1**. For typical synthesis of TiO_2 flowers, 5 ml Ti (IV) tetra isopropoxide (TTIP) is poured into 20 ml of water in ice-cold condition to form white precipitate of titanium hydroxide. Hydrochloric acid is then added drop wise in the solution under stirring condition until the precipitate is dissolved completely to form a transparent solution. Cetyl trimethyl-ammonium bromide (CTAB) is added to the clear solution and stirred for another 30 min. Spherical carbon templates (diameter in the range 2–2.5 μm) are then added into the mixture. The spherical carbon templates are derived from sucrose through hydrothermal synthesis route described elsewhere (Mukherjee and Majumder, 2012). The whole mixture is kept under ultra-sonication for 15 min and then transferred in a teflon-lined stainless steel autoclave. The autoclave is heated at 180°C for 8 h and cooled thereafter in air at ambient temperature. Resulting product is centrifuged and washed repeatedly with water and ethanol to achieve white mass. The product is dried at 80°C for 24 h and then calcined at 450°C for 2 h to achieve flower like architecture composed of TiO_2 nano-rods.

Synthesis of Pt Nano-Particles and Pt Modified TiO_2 Flower Like Structure (Ti-Nr-Pt)

Pt nano-particles are synthesized separately by the chemical reduction of hexachloroplatinic acid ($H_2PtCl_6.2H_2O$) using sodium borohydride ($NaBH_4$). First 50 mg of $H_2PtCl_6.2H_2O$ is dissolved in 100 ml of water within a round bottom flask. $NaBH_4$ and CTAB are added as reducing agent and surfactant, respectively to the aqueous solution of $H_2PtCl_6.2H_2O$. The mixture is refluxed at 110°C for 2h in N_2 atmosphere to achieve dark brown residue which resulted black mass after centrifugation. The black mass is repeatedly washed with distilled water and finally using ethanol to remove the dissolved inorganics and surfactants. The synthesized Pt nano-particles are finally dispersed with the synthesized TiO_2 flowers ultrasonically for 1 h to obtain the Pt modified flower like TiO_2 architecture (Ti-Nr-Pt).

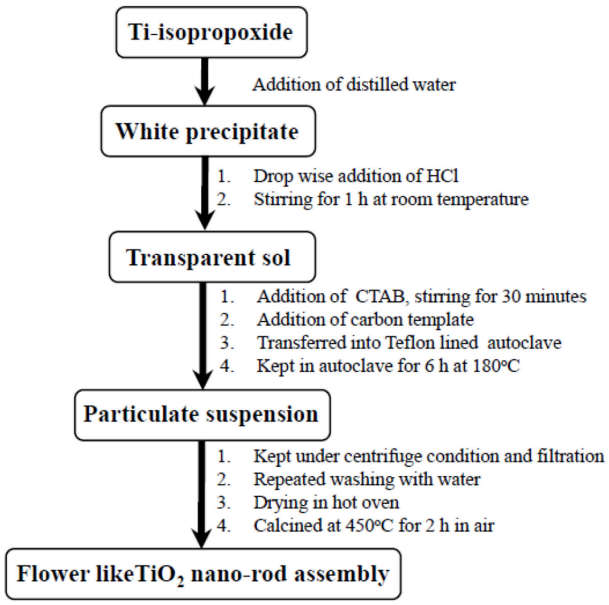

FIGURE 1 | Flow diagram for synthesis of flower like TiO_2 nano-rod assembly.

Phase and Morphological Characterizations of the Synthesized Materials

The crystalline nature of the synthesized Ti-Nr samples is studied using X-ray diffractometer (XRD) (PW 3040/60, Panalytical, Netherland). The morphologies of Ti-Nr and Ti-Nr-Pt samples are studied using field emission scanning electron microscope (FESEM) (Σigma HD, Zeiss, Germany) and transmission electron microscope (TEM) (JEM 2100, Jeol Ltd., Japan). The energy dispersive X-ray spectra (EDS), lattice fringe pattern and selected area electron diffraction patterns of Ti-Nr and Ti-Nr-Pt samples are acquired from transmission electron microscope.

Preparation of Sensing Elements and Protocols for Sensing Measurements

Thick films of Ti-Nr and Ti-Nr-Pt samples are coated on alumina substrate using a mixture of ethyl cellulose and terpineol to prepare the sensing element. The alumina substrate having thickness ∼2 mm was procured from ANTS Ceramic Pvt. Ltd. To prepare the thick film of Ti-Nr and Ti-Nr-Pt nano particles, a binder was prepared by mixing ethyl cellulose and terpineol (weight ratio 1:10) at 60°C to make a viscous liquid. Next, the prepared samples were ultrasonicated with ethanol for ∼30 min and then the binder was mixed with this ultrasonicated mixture of TiO_2 samples to make a smooth paste. Finally the paste of the TiO_2 samples were spread over the alumina substrate by doctor blade technique to prepare the thick films. Here, the role of ethyl cellulose and terpineol is to be used as a binder which helps to create the inter particle contact of the prepared materials and also it makes the good adhesion of the samples over the alumina substrate. The coated alumina substrates are heat treated at 400°C for 1 h to remove the organics. Silver paste based strip electrodes (separated by ∼2 mm) are prepared on their surface to measure the current response of prepared sensing elements. Sensing characteristics are measured using a static flow gas sensing measurement set-up developed in the laboratory. The details of the set-up have already been described elsewhere (Das et al., 2017a). The sensing characteristics are measured by varying the operating temperature (225–300°C) of the sensor and concentration (10–200 ppm) of isopropanol. Sensing elements are kept at the respective operating temperature for ∼30 min to achieve a constant current response in air (I_0) prior to perform the experiments. During the sensing measurements, the surface current of the sensor is measured by applying a fixed voltage (∼20 V) on one of the electrode. The sensitivity (S) of the sensor is estimated by measuring the change of current (ΔI) during sensing with respect to its initial value of current (I_0) using following relationship (Equation 1).

$$S = \Delta I / I_0 \quad (1)$$

RESULTS AND DISCUSSIONS

Phase and Morphological Features of Synthesized Materials

The FESEM image of the prepared carbon sphere templates is shown in the **Figure 2a**. As indicated from the figure, the sizes of the spheres are homogenous having diameter in the range of 2–2.5 μm. Surface of these carbon spheres possess hydrophilic C=O and –OH groups which act as nucleation center for the growth of metal oxide nano-structures (Das et al., 2016). **Figures 2b–d** shows the typical FESEM images of Ti-Nr samples at different magnifications. The acentric growth of nano-rods to form flower like structure is reflected in FESEM images. It is predicted here that spherical morphology of the carbon template facilitates the growth of TiO_2 flower like architecture. The plausible mechanism for the formation of the said flower like architecture is represented in **Figure 2e**. In presence of HCl, initially TTIP hydrolyses in the reaction medium and forms ($Ti(OC_4H_9)_{4-m-n}(OH)_mCl_n$) complex where m and n are the stoichiometry of the associated hydroxyl group (OH^-) and chloride (Cl^-) ion. During hydrothermal condition the said complex dissociates and forms TiO_2 nucleation center. The HCl medium here controls the hydrolysis of TTIP and rate for the nucleation of TiO_2 nano-rods. Pottier et al. reported that the formation of rutile phase titania is promoted in HCl environment (Pottier et al., 2001). CTAB plays the important role for the growth of nucleation centers by preventing their agglomeration.

Typical TEM micrographs of Ti-Nr samples are shown in **Figures 3a,b** where flower like architecture composed of TiO_2 nano-rods is distinguished clearly. The polycrystalline nature of the samples is confirmed in the SAED pattern shown in inset of **Figure 3b**. The patterns are indexed as rutile TiO_2 by matching the calculated "d" spacing with standard JCPDS (Card No. 86-0147). The arrangement of each TiO_2 nano-rod with nib like end is identified in the TEM image shown in **Figure 3c**. The length and width of individual nano-rods are found in the range of 60–65 and 25–27 nm respectively. The lattice fringes shown in the

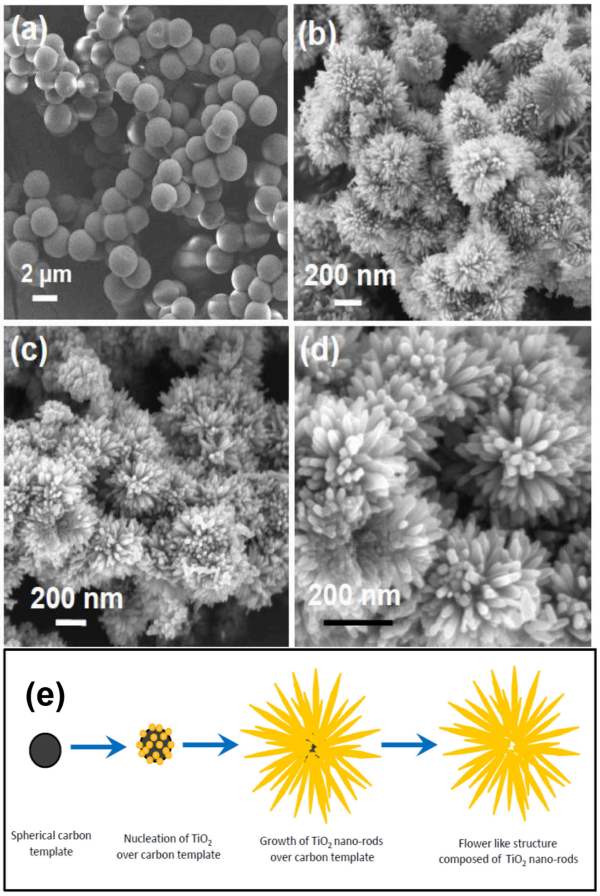

FIGURE 2 | (a) Surface morphology of synthesized carbon sphere templates. **(b–d)** FESEM images of flower like TiO_2 nano-rod assembly (Ti-Nr) at different magnification. **(e)** Plausible mechanism for the formation of Ti-Nr structure.

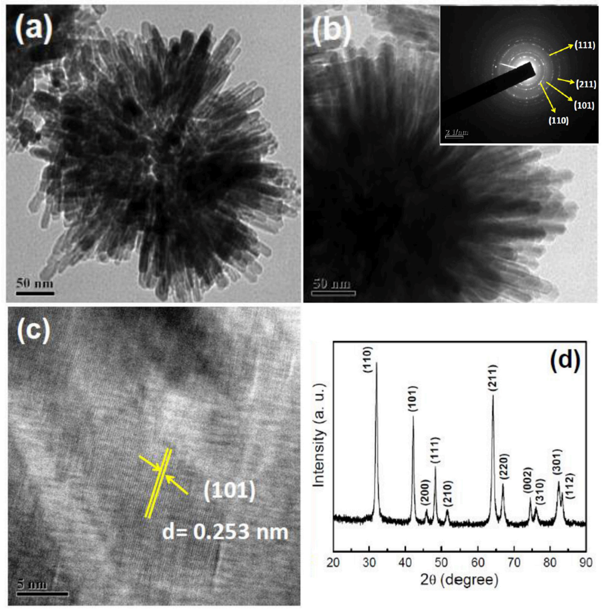

FIGURE 3 | TEM images of Ti-Nr structure at **(a)** low and **(b)** high magnification. Inset of Figure **(b)** SAED pattern of Ti-Nr sample. **(c)** Lattice fringe and **(d)** X-ray diffraction pattern of rutile Ti-Nr particles.

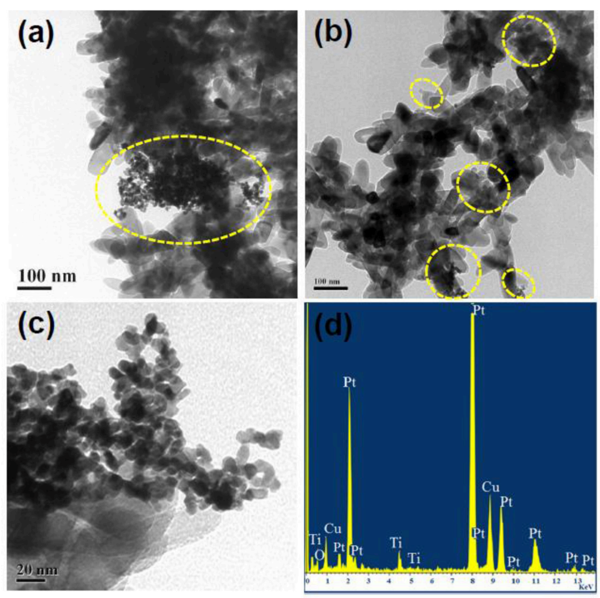

FIGURE 4 | (a,b) TEM images of Pt modified flower like TiO_2 (Ti-Nr-Pt) samples. **(c)** Enlarged view of Pt nano-particles within Ti-Nr-Pt sample. **(d)** EDS of Ti-Nr-Pt sample.

TEM image of the nano-rods are representing the (101) plane of rutile phase TiO_2. The rutile crystal structure of synthesized Ti-Nr samples is further confirmed from the X-ray diffraction (XRD) pattern represented in **Figure 3d**. The diffraction peaks match well with the standard rutile phase TiO_2.

Figures 4a,b represent the TEM images of Ti-Nr-Pt samples where Pt nano-particles are distributed over TiO_2 nano-rods. **Figure 4c** shows enlarged view of the Pt particles within the size range of 5–8 nm. The presence of Pt, Ti, O elements in the composition of Ti-Nr-Pt is confirmed in the EDS presented in **Figure 4d**. The peaks for Cu arise from copper grid which has been used as substrate for TEM study. The low magnification tilted view of SEM micrograph of the TiO_2 thick film is shown in the **Figure 5**. The thickness of TiO_2 thick film is in the range of 50–55 μm and it is uniformly coated on the alumina substrate.

Chemi-Resistive Sensing Characteristics

In chemi-resistive gas/vapor sensors, the resistance/conductance of a sensing element changes in exposure of reducing/oxidizing vapors. The principle of sensing mechanism is illustrated well by researchers (Franke et al., 2006). However, for the ease of understanding to the readers, the schematic sensing mechanism for nano-rod like structure is presented briefly in **Figure 6A**. The SMO based chemi-resistive sensors operate generally at elevated temperature at which atmospheric O_2 is first chemi-adsorbed on the surface of the sensing element. Here,

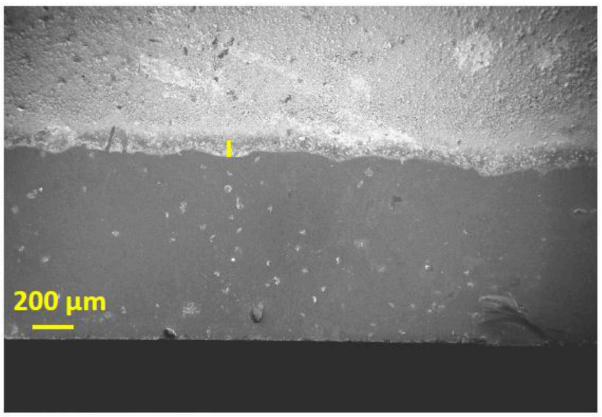

FIGURE 5 | SEM micrograph of TiO_2 thick film of thickness 50-55 µm.

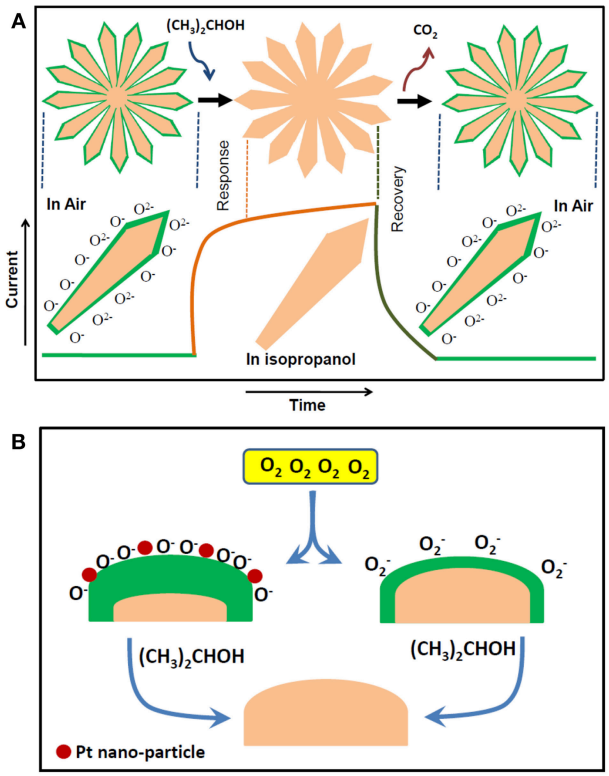

FIGURE 6 | Schematic representation of **(A)** isopropanol sensing phenomenon over flower like architecture comprised of TiO_2 nano-rods (Ti-Nr). **(B)** Sensitization of sensing surface by Pt nano-particles for chemi-adsorption of atomic oxygen.

the chemi-adsorption represents the phenomenon of electron trapping from the conduction band of SMOs by atmospheric oxygen. Depending on the temperature of the sensing element, oxygen may chemi-adsorbed in the atomic/molecular form which is described in Equation (2). Such chemi-adsorbed oxygen develop electronically depleted layer on sensor surface and forms Schottky potential barrier for electron conduction leading to decrease in sensor's electrical conductance. Chemi-adsorbed oxygens then oxidize the exposed reducing vapor (e.g., isopropanol) and release the trapped electrons back to the conduction band of the sensor. As a consequence, the value of surface current for "n" type SMO sensor increases. The reaction of chemi-adsorbed oxygen with isopropanol vapor on sensor surface is presented in Equations (3, 4) (Kulkarni and Wachs, 2002). Sequential change in the surface current of flower like TiO_2 architecture due to the formation and decay of electron depleted layer when it is switching back and forth between oxygen and isopropanol at elevated temperature is illustrated in the figure.

$$O_2(\text{atmospheric}) + e^- \rightarrow O_2^-/2O^-(\text{chemi} - \text{adsorbed}) \quad (2)$$

$$(CH_3)_2CHOH_{ad} + O_2^-/O^- \rightarrow (CH_3)_2CO_{ad} + H_2O_{ad} + e^- \quad (3)$$

$$(CH_3)_2CO_{ad} + H_2O_{ad} \rightarrow CO_2(g) + H_2O(g) \quad (4)$$

Noble metal nano-particles (e.g., Pt nano-particles) on SMO surface expedite the transformation of molecular oxygen to atomic oxygen (**Figure 6B**) which is known as "spillover effect" (Cao et al., 2008). As a consequence, larger amount of electrons is trapped by atomic oxygen than molecular oxygen leading to the higher depletion width for Ti-Nr-Pt than its unmodified counterpart. Likewise, the reaction of reducing vapor (e.g., isopropanol) with chemi-adsorbed atomic oxygen (O^-) will release more electrons than chemi-adsorbed molecular oxygen resulting higher change of electrical conductance of Ti-Nr-Pt than Ti-Nr.

In the forthcoming discussion, operating temperature and gas concentration dependent sensing performances of Ti-Nr and Ti-Nr-Pt based sensing elements are described. The current response transients of both Ti-Nr and Ti-Nr-Pt sensor for the detection of 200 ppm isopropanol at 250 and 275°C are shown in **Figures 7A–D**, respectively. As reflected from the figures, the current response of both Ti-Nr and Ti-Nr-Pt sensors gradually increases with time due to interaction with isopropanol and ultimately saturates. The sensitivity (S) of the sensors Ti-Nr and Ti-Nr-Pt is found 3.0 and 7.0, respectively for the detection of 200 ppm isopropanol at 275°C. The promising isopropanol sensing of both Ti-Nr and Ti-Nr-Pt samples are confirmed in **Figures 7A–D**. However, comparing the figures it is stated that the sensitivity of Ti-Nr-Pt sample toward isopropanol is higher than Ti-Nr.

The operating temperature dependent sensitivity of Ti-Nr and Ti-Nr-Pt samples for the detection of 200 ppm isopropanol is presented in **Figure 7E**. Higher sensitivity of Ti-Nr-Pt than Ti-Nr is observed in the entire operating temperature range (225–300°C). It is notable here that for both the samples, sensitivity first increases with operating temperature, attains maximum and then decreases leading to maximum sensitivity at an optimum temperature. The optimum operating temperature of both Ti-Nr and Ti-Nr-Pt samples for the detection of isopropanol is observed at ~ 275°C. Similar change of sensitivity with operating temperature is generic for other SMO based chemi-resistive sensors (Barsan and Tomescu, 1995; Das et al., 2017b). The

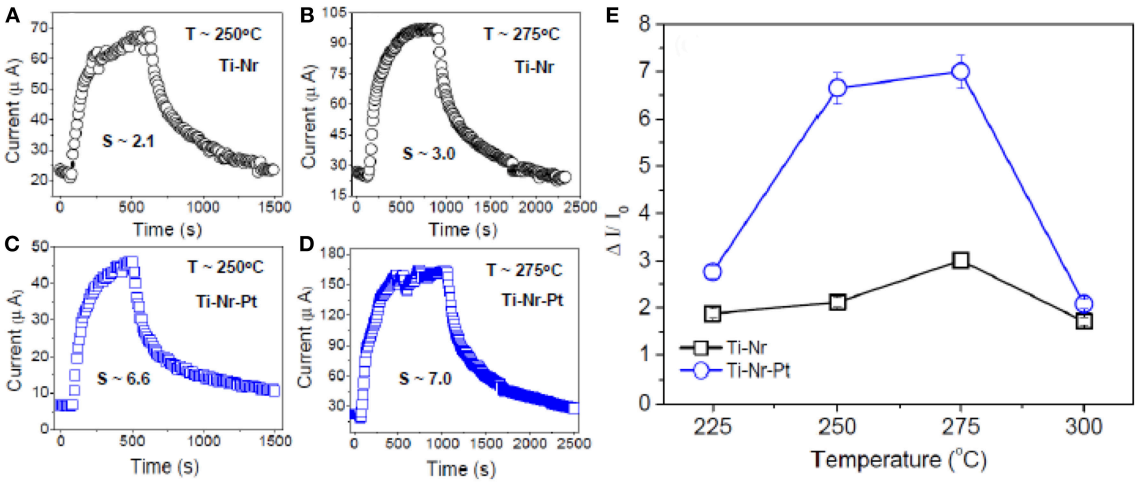

FIGURE 7 | Typical current transients for **(A,B)** Ti-Nr and **(C,D)** Ti-Nr-Pt sensor for the detection of 200 ppm isopropanol at 250° and 275°C, respectively. The sensitivity values are mentioned in the figure. **(E)** Operating temperature (range 225–300°C) dependent sensitivity of both the sensors toward 200 ppm isopropanol.

maximum sensitivity for SMO sensors at an optimum operating temperature can be explained using the concept of depleted layer width and the larger desorption of vapors at high temperature. The initial rise of sensitivity (S) with operating temperature can be explained using the following relationship of sensitivity (S) with depletion layer width (L_D) and charge carrier concentration (Equations 5, 6).

$$L_D = (\varepsilon_o KT/n_o e^2)^{1/2} \quad (5)$$

$$S = \Delta G/G_o = (\Delta n/n_o)L_D \quad (6)$$

where ε_o is the static dielectric constant, n_o is the total carrier concentration, e is the carrier charge, K is the Boltzmann constant, T is the absolute temperature, Δn is the change in the carrier concentration.

The electrical conductance as well as charge carrier concentration of SMO sensors increases with the rise in operating temperature and thus from the aforementioned relationships, it can be stated that the maximum response of the sensor will be obtained at an optimum operating temperature. The enhanced desorption of vapors at sufficiently high temperature results poor gas-solid interaction which predominates over the increase of charge career concentration leading to decreased sensitivity. The higher sensitivity of Ti-Nr-Pt than Ti-Nr due to the formation of wider depleted layer and larger change of charge carrier concentration can also be described by Equation (5). The current response transients of Ti-Nr and Ti-Nr-Pt samples for the detection of 10–100 ppm isopropanol (at optimum operating temperature ~275°C) are presented in **Figures 8A,B** respectively. Comparing the figures, it is observed that Ti-Nr-Pt samples shows better sensitivity than Ti-Nr within the studied concentration range. In order to compare the kinetics for the change of sensitivity of Ti-Nr-Pt and Ti-Nr sensors for the detection of isopropanol, the current response transients of both the sample are modeled in accordance to Langmuir Hinshelwood reaction mechanism. The reaction of isopropanol with chemi-adsorbed molecular or atomic oxygen over Ti-Nr and Ti-Nr-Pt (described in Equation 3) sensors is reflected through the current response transients. As the reaction of isopropanol with chemi-adsorbed oxygen progresses, the current response of sensor also increases with time. On the way to model the current response transient of the sensor in accordance to the reaction presented in Equation (3), it is assumed that the site fraction θ is covered by reaction product ($(CH_3)_2CO_{ad}$) and the rest available unoccupied sites (F- θ) are occupied by chemi-adsorbed oxygen (O^- or O_2^-) on the sensor surface. Here, full surface coverage site is considered as F and rate constant of this reaction is defined as k_a. The rate of formation of the product considering the reaction mentioned in Equation (3) is thus can be described by the following relation:

$$d[(CH_3)_2CO_{ad}]/dt = k_a[O_{ad}^-/O_{2ad}^-][(CH_3)_2CHOH_{ad}] \quad (7)$$

Rewriting Equation (7) in terms of respective site occupancies

$$d\theta/dt = k_a[F - \theta]C_g \quad (8)$$

Assuming full adsorption of low concentration (C_g) of $(CH_3)_2CHOH$, thus $[(CH_3)_2CHOH_{ad}] \sim C_g$, Solving Equation (8) one can write

$$d[(CH_3)_2CO_{ad}]/dt = F(1 - \exp^{-(kaCgt)}) \quad (9)$$

The maximum sensitivity of the sensor corresponds to the situation when all its active sites (F) are occupied by the reaction product $[(CH_3)_2CO_{ad}]$. Therefore the transient sensitivity (S(t)) can be expressed by the following relation.

$$S(t) = S_{max}(1 - \exp^{-(k_a c_g t)}) \quad (10)$$

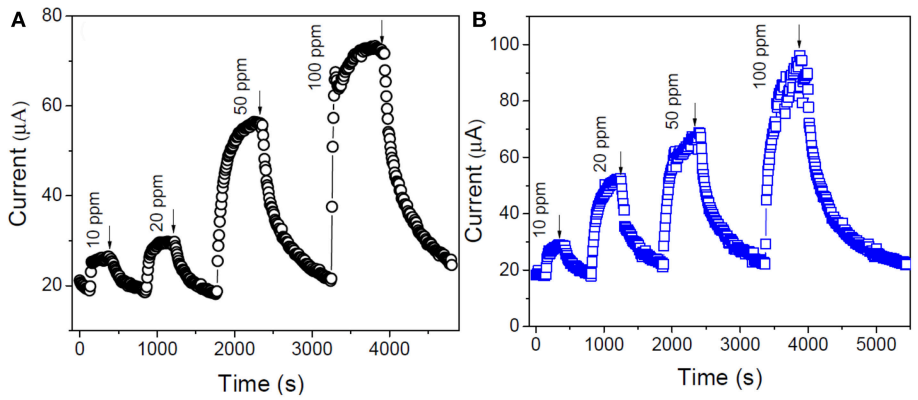

FIGURE 8 | Typical current response transients for **(A)** Ti-Nr and **(B)** Ti-Nr-Pt sensor for the detection of 10-100 ppm isopropanol at 275°C.

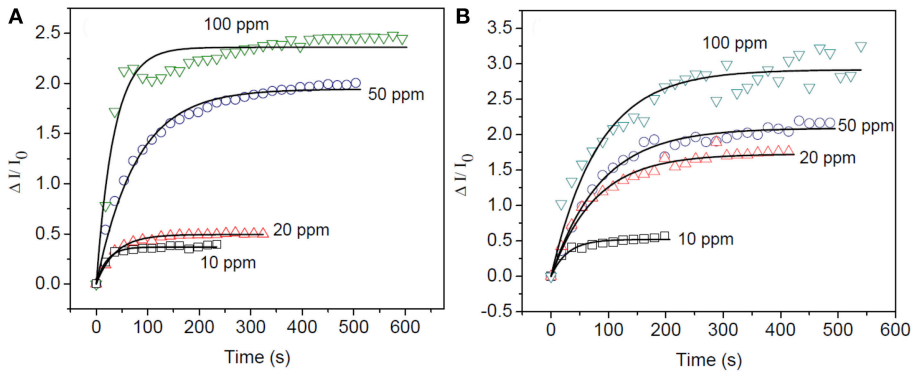

FIGURE 9 | Modeling of transient sensitivity of **(A)** Ti-Nr and **(B)** Ti-Nr-Pt samples for the detection of 10-100 ppm of isopropanol in accordance to Langmuir Hinshelwood mechanism.

Figures 9A,B represents the time dependent sensitivity plot of Ti-Nr and Ti-Nr-Pt for the detection of 10–100 ppm of isopropanol as well as their modeling in accordance to Equation (10). It is notable from the figure that at lower concentration ($\leq$ 50 ppm), the model fits well with the experimental results. However, the model is observed deviated at higher vapor concentration ($\sim$100 ppm). The values of sensitivity, time constants and rate constants for the sensing of isopropanol are estimated from the fitting (summarized in **Table 1**). As estimated, the time constant increases and the rate of the reaction lowers with the rise in isopropanol concentration. The rate for the sensing of isopropanol over Ti-Nr-Pt is also found slower as compared to the sensing over Ti-Nr sample. The decay of wider depletion layer by the released electron due to the oxidation of isopropanol over Ti-Nr-Pt samples takes longer time as compared over Ti-Nr which is reflected in the values of time constant and rate constant in **Table 1**. The improvement of the value of sensitivity or response on the noble metal modified SMO surface is reported in literature (Kolmakov et al., 2005; Dolbec et al., 2007; Xiang et al., 2010; Jang et al., 2013). However, comparative study regarding the kinetics for the sensing of vapors over primitive and noble metal modified SMO surface can hardly found in open literature.

TABLE 1 | Kinetic parameters estimated from the fitting of transient sensitivity of Ti-Nr and Ti-Nr-Pt samples for the detection of 10–50 ppm isopropanol.

Sample	Conc^n (ppm)	S_{max}	τ (s)	k_a (s^{-1})
(Ti-Nr)	10	0.37	20	0.05
	20	0.49	37	0.027
	50	1.94	78	0.128
(Ti-Nr-Pt)	10	0.52	28	0.035
	20	1.72	76	0.0131
	50	2.09	85	0.0117

CONCLUSION

In the present study, flower like architecture comprised of innumerable numbers of TiO_2 nano-rods (Ti-Nr samples) are synthesized hydrothermally and thereafter modified chemically with Pt nano-particles (Ti-Nr-Pt samples). The plausible mechanism for the spherical carbon template mediated hydrothermal growth of Ti-Nr samples is described. The synthesized materials are characterized in terms of their phase formation behavior and morphological features. The Ti-Nr

samples are identified as rutile phase by analyzing the X-ray diffraction patterns. The scanning/transmission electron microscope images along with the associated energy dispersive X-ray spectrum and selected area electron diffraction patterns are used to evaluate the morphology and crystalline nature of the samples. As observed, micron size flowers are composed of eccentrically grown vertically aligned TiO_2 nano-rods which provide larger surface area for the chemi-adsorption of oxygen and facilitate better interaction with isopropanol. The chemi-resistive type sensing toward isopropanol for both Ti-Nr and Ti-Nr-Pt sensors are investigated in a static flow reactor unit developed in the laboratory. The operating temperature (225–300°C) of sensing materials and concentration (10–200 ppm) of isopropanol are varied to measure the sensitivity of the prepared materials. It is found that both the Ti-Nr and Ti-Nr-Pt sensors show promising response toward isopropanol. The optimum sensing performances for both the samples are observed at ∼275°C. The Pt modified Ti-Nr-Pt samples however show better sensitivity than the unmodified Ti-Nr samples within the range of studied operating temperature. The sensitivity at optimum operating temperature ∼275°C for Ti-Nr and Ti-Nr-Pt sensors toward the detection of 10 ppm isopropanol is found 0.37 and 0.52, respectively. The formation of wider depleted layer by chemi-adsorbed oxygen, generation of more electrons during the interaction of isopropanol on Ti-Nr-Pt sensor leads to the better sensitivity as compared to Ti-Nr sensor. The current response transients of Ti-Nr and Ti-Nr-Pt sensors are modeled in accordance to Langmuir-Hinshelwood mechanism in order to understand their kinetics for sensing low concentration (10–50 ppm) of isopropanol. The characteristic time constants for both the samples for sensing isopropanol increase with the rise in isopropanol concentration. The rate constant for the decay of depletion layer due to the interaction of isopropanol with atomic oxygen over Ti-Nr surface is found larger than the same interaction with molecular oxygen over Ti-Nr-Pt surface.

DATA AVAILABILITY

All datasets generated for this study are included in the manuscript.

AUTHOR CONTRIBUTIONS

PD: conceptualization, data acquisition, methodology, analysis, and writing-original draft; BM: conceptualization, supervision, and writing-review and editing; KM: conceptualization, analysis, supervision, writing-review and editing, and funding acquisition.

ACKNOWLEDGMENTS

The author KM is thankful to DST, Govt. of India for providing him Inspire Faculty fellowship (Ref. DST/IFA12-CH-43) and associated research grant for this work. PD is thankful to DST, Govt. of India for supporting her fellowship. KM has partly spent time in analyzing the data, preparing and communicating the manuscript as Fulbright Nehru Postdoc Fellow from his present affiliation George Washington University, USA.

REFERENCES

Bai, J., and Zhou, B. (2014). Titanium dioxide nanomaterials for sensor applications. *Chem. Rev.* 114, 10131–10176. doi: 10.1021/cr400625j

Barsan, N., and Tomescu, A. (1995). The temperature dependence of the response of SnO_2-based Gas Sensing Layers to O_2, $CH_4$and CO. *Sens. Actuator B-Chem.* 26, 45–48. doi: 10.1016/0925-4005(94)01553-T

Bhowmik, B., and Bhattacharyya, P. (2015). Highly stable low temperature alcohol sensor based on hydrothermally grown tetragonal titania nanorods. *RSC Adv.* 5, 82159–82168. doi: 10.1039/C5RA14518J

Cao, M., Wang, Y., Chen, T., Antonietti, M., and Niederberger, M. (2008). A highly sensitive and fast-responding ethanol sensor based on $CdIn_2O_4$ nanocrystals synthesized by a nonaqueous Sol-Gel Route. *Chem. Mater.* 20:5781–5786. doi: 10.1021/cm800794y

Damodaran, V. B., Bhatnagar, D., Leszczak, V., and Popat, K. C. (2015). Titania nanostructures: a biomedical perspective. *RSC Adv.* 5:37149. doi: 10.1039/C5RA04271B

Das, P., Mondal, B., and Mukherjee, K. (2016). Hierarchical Zinc Oxide nano-tips and micro-rods: hydrothermal synthesis and improved chemiresistive response towards ethanol. *RSC Adv.* 6:1408. doi: 10.1039/C5RA23203A

Das, P., Mondal, B., and Mukherjee, K. (2017a). Simultaneous adsorption-desorption processes in the conductance transient of anatase titania for sensing ethanol: a distinctive feature with kinetic perception. *J. Phys. Chem. C.* 121, 1146–1152. doi: 10.1021/acs.jpcc.6b10041

Das, P., Mondal, B., and Mukherjee, K. (2017b). Chemi-resistive response of rutile titania nano-particles towards isopropanol and formaldehyde: a correlation with the volatility and chemical reactivity of vapors. *Mater. Res. Exp.* 4:015503. doi: 10.1088/2053-1591/4/1/015503

Dolbec, R., and E. I., Khakani, M. A. (2007). Sub-ppm sensitivity towards carbon monoxide by means of pulsed laser deposited SnO_2:Pt Based Sensors. *Appl. Phys. Lett.* 90:173114. doi: 10.1063/1.2731710

Dong, C., Liu, X., Xiao, X., Chen, G., Wang, Y., and Djerdj, I. (2014). Combustion synthesis of porous pt-functionalized SnO_2 sheets for isopropanol gas detection with a significant enhancement in response. *J. Mater. Chem. A.* 2:20089. doi: 10.1039/C4TA04251D

Epifani, M., Helwig, A., Arbiol, J., Díaz, R., Francioso, L., Siciliano, P., et al. (2008). TiO_2 Thin Films from titanium butoxide: synthesis, pt addition, structural stability, microelectronic processing and gas-sensing properties. *Sens. Actuator B Chem.* 130, 599–608. doi: 10.1016/j.snb.2007.10.016

Franke, M. E., Koplin, T. J., and Simon, U. (2006). Metal and metal oxide nanoparticles in chemiresistors: does the nanoscale matter? *Small.* 2:36. doi: 10.1002/smll.200500261

Hotovy, I., Huran, J., Siciliano, P., Capone, S., Spiessd, L., and Rehacek, V. (2004). Enhancement of H_2 sensing properties of NiO-based thin films with a pt surface modification. *Sens. Actuator B Chem.* 103, 300–311. doi: 10.1016/j.snb.2004.04.109

Hu, P., Du, G., Zhou, W., Cui, J., Lin, J., Liu, H., et al. (2010). Enhancement of ethanol vapor sensing of TiO_2 nanobelts by surface engineering. *ACS Appl. Mater. Interfaces* 2:3263. doi: 10.1021/am100707h

Jammalamadaka, D., and Raissi, S. (2010). Ethylene glycol, methanol and isopropyl alcohol intoxication. *Am. J. Med. Sci.* 339, 276–281. doi: 10.1097/MAJ.0b013e3181c94601

Jang, B. H., Landau, O., Choi, S. J., Shin, J., Rothschild, A., and Kim, I. D. (2013). Selectivity Enhancement of SnO_2 nanofiber gas sensors by functionalization with pt nanocatalysts and manipulation of the operation temperature. *Sens. Actuator B Chem.* 188, 156–168. doi: 10.1016/j.snb.2013.07.011

Kolmakov, A., Klenov, D. O., Lilach, Y., Stemmer, S., and Moskovits, M. (2005). Enhanced gas sensing by individual SnO_2 nanowires and nanobelts functionalized with Pd catalyst particles. *Nano Lett.* 5, 667–673. doi: 10.1021/nl050082v

Kulkarni, D., and Wachs, I. E. (2002). Isopropanol oxidation by pure metal oxide catalysts: number of active surface sites and turnover frequencies. *Appl. Catal. A.* 237, 121–137. doi: 10.1016/S0926-860X(02)00325-3

Lakshmi, B. B., Dorhout, P. K., and Martin, C. R. (1997). Sol-Gel template synthesis of semiconductor nanostructures. *Chem. Mater.* 9, 857–862.

Lao, J. Y., Wen, J. G., and Ren, Z. F. (2002). Hierarchical ZnO nanostructures. *Nano Lett.* 2, 1287–1291. doi: 10.1021/nl025753t

Lee, J., Kim, D. H., Hong, S. H., and Jho, J. Y. (2011). A hydrogen gas sensor employing vertically aligned TiO_2 nanotube arrays prepared by template-assisted method. *Sens. Actuator B Chem.* 160, 1494–1498. doi: 10.1016/j.snb.2011.08.001

Li, K., Li, B., Wu, J., Kang, F., Kim, J. K., and Zhang, T. Y. (2017). Ultrafast-charging and long-life li-ion battery anodes of TiO_2-B and anatase dual-phase nanowires. *ACS Appl. Mater. Interfaces* 9, 35917–35926. doi: 10.1021/acsami.7b11652

Mao, Y., and Wong, S. S. (2004). General room-temperature method for the synthesis of isolated as well as arrays of single-crystalline ABO_4-type nanorods. *J. Am. Chem. Soc.* 126, 15245–15252. doi: 10.1021/ja046331j

Mukherjee, K., and Majumder, S. B. (2012). Promising methane sensing characteristics of hydrothermal synthesized magnesium zinc ferrite hollow sphere. *Scr. Mater.* 67, 617–620. doi: 10.1016/j.scriptamat.2012.06.025

Mukherjee, K., and Majumder, S. B. (2013). Synthesis of embedded and isolated $Mg_{0.5}Zn_{0.5}Fe_2O_4$ nano-tubes and investigation on their anomalous gas sensing characteristics. *Sens. Actuator B Chem.* 177, 55–63. doi: 10.1016/j.snb.2012.10.108

O'Regan, B., and Grätzel, M. (1991). A low-cost, high-efficiency solar cell based on dye-sensitized colloidal TiO_2 Films, *Nature.* 353, 737–740.

Park, N. G., J., and van de Lagemaat, Frank, A. J. (2000). Comparison of dye-sensitized rutile- and anatase-based TiO_2 Solar Cells. *J. Phys. Chem. B.* 104, 8989–8994. doi: 10.1021/jp994365l

Pottier, A., Chanéac, C., Tronc, E., Mazerolles, L., and Jolivet, J. P. (2001). Synthesis of brookite TiO_2 nanoparticles by thermolysis of $TiCl_4$ in strongly acidic aqueous media. *J. Mater. Chem.* 11, 1116–1121. doi: 10.1039/b100435m

Schneider, J., Matsuoka, M., Takeuchi, M., Zhang, J., Horiuchi, Y., Anpo, M., et al. (2014). Understanding TiO_2 photocatalysis: mechanisms and materials. *Chem. Rev.* 114, 9919–9986. doi: 10.1021/cr5001892

Shi, J., and Wang, X. (2011). Growth of rutile titanium dioxide nanowires by pulsed chemical vapor deposition. *Cryst. Growth Des.* 11, 949–954. doi: 10.1021/cg200140k

Sun, X., Liu, J., and Li, Y. (2006). Use of carbonaceous polysaccharide microspheres as templates for fabricating metal oxide hollow spheres. *Chem. Eur. J.* 12:2039. doi: 10.1002/chem.200500660

Tian, Z. R., Voigt, J. A., Liu, J., Mckenzie, B., and Xu, H. (2003). Large oriented arrays and continuous films of TiO_2-based nanotubes. *J. Am. Chem. Soc.* 125, 12384–12385. doi: 10.1021/ja0369461

Titirici, M. M., Antonietti, M., and Thomas, A. (2006). A generalized synthesis of metal oxide hollow spheres using a hydrothermal approach. *Chem. Mater.* 18, 3808–3812. doi: 10.1021/cm052768u

Wang, C., Yin, L., Zhang, L., Qi, Y., Lun, N., and Liu, N. (2010). Large scale synthesis and gas-sensing properties of anatase tio_2 three-dimensional hierarchical nanostructures. *Langmuir* 26, 12841–12848. doi: 10.1021/la100910u

Wang, D., Zhou, W., Hu, P., Guan, Y., Chen, L., Li, J., et al. (2012). High ethanol sensitivity of Palladium/TiO_2 nanobelt surface heterostructures dominated by enlarged surface area and nano-schottky junctions. *J. Colloid Interface Sci.* 388, 144–150. doi: 10.1016/j.jcis.2012.08.034

Xiang, Q., Meng, G. F., Zhao, H. B., Zhang, Y., Li, H., Ma, W. J., et al. (2010). Au Nanoparticle Modified WO_3 nanorods with their enhanced properties for photocatalysis and gas sensing. *J. Phys. Chem. C.* 114, 2049–2055. doi: 10.1021/jp909742d

Yurdakal, S., Palmisano, G., Loddo, V., Augugliaro, V., and Palmisano, L. (2008). Nanostructured rutile TiO_2 for selective photocatalytic oxidation of aromatic alcohols to aldehydes in water. *J. Am. Chem. Soc.* 130, 1568–1569. doi: 10.1021/ja709989e

Zhou, X., Liu, N., and Schmuki, P. (2017). Photocatalysis with TiO_2 Nanotubes: "Colorful" reactivity and designing site-specific photocatalytic centers into TiO_2 Nanotubes. *ACS Catal.* 7, 3210–3235. doi: 10.1021/acscatal.6b03709

Conflict of Interest Statement: The authors declare that the research was conducted in the absence of any commercial or financial relationships that could be construed as a potential conflict of interest.